JACS
JOURNAL OF THE AMERICAN CHEMICAL SOCIETY

Subscriber access provided by ISTANBUL TEKNIK UNIV

Article

Guest-Induced Modification of a Magnetically Active Ultramicroporous, Gismondine-like, Copper(II) Coordination Network

Jorge A. R. Navarro, Elisa Barea, Antonio Rodrguez-Diguez, Juan M. Salas, Conchi O. Ania, Jos B. Parra, Norberto Masciocchi, Simona Galli, and Angelo Sironi

J. Am. Chem. Soc., **2008**, 130 (12), 3978-3984 • DOI: 10.1021/ja078074z

Downloaded from http://pubs.acs.org on February 8, 2009

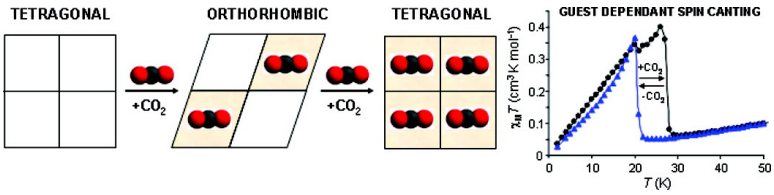

More About This Article

Additional resources and features associated with this article are available within the HTML version:

- Supporting Information
- Links to the 4 articles that cite this article, as of the time of this article download
- Access to high resolution figures
- Links to articles and content related to this article
- Copyright permission to reproduce figures and/or text from this article

View the Full Text HTML

ACS Publications
High quality. High impact.

Journal of the American Chemical Society is published by the American Chemical Society. 1155 Sixteenth Street N.W., Washington, DC 20036

J|A|C|S
ARTICLES
Published on Web 03/06/2008

Guest-Induced Modification of a Magnetically Active Ultramicroporous, Gismondine-like, Copper(II) Coordination Network

Jorge A. R. Navarro,*[,†] Elisa Barea,[‡] Antonio Rodríguez-Diéguez,[§] Juan M. Salas,[†] Conchi O. Ania,[||] José B. Parra,*[,||] Norberto Masciocchi,[⊥] Simona Galli,[⊥] and Angelo Sironi*[,§]

Departamento de Química Inorgánica, Universidad de Granada, Av. Fuentenueva S/N, 18071 Granada, Spain, Dipartimento di Chimica Inorganica, Metallorganica e Analitica, Università degli Studi di Milano, Via Venezian 21, 20133 Milan, Italy, Dipartimento di Chimica Strutturale e Stereochimica Inorganica, Università degli Studi di Milano and ISTM-CNR, Via Venezian 21, 20133 Milan, Italy, Department of Energy & Environment, Instituto Nacional del Carbón, CSIC, Apartado 73, 33080 Oviedo, Spain, and Dipartimento di Scienze Chimiche e Ambientali, Università dell'Insubria, Via Valleggio 11, 22100 Como, Italy

Received October 22, 2007; E-mail: jarn@ugr.es; jbparra@incar.csic.es; angelo.sironi@istm.cnr.it

Abstract: A novel ultramicroporous coordination polymer, namely $[Cu(F\text{-pymo})_2(H_2O)_{1.25}]_n$ (**1**, F-pymo = 5-fluoropyrimidin-2-olate), has been prepared and structurally characterized. **1** displays a zeolitic gismondine (GIS) topology, with ca. 2.9 Å wide helical channels which, in the thermally activated counterpart (**1′**), account for a 13% void volume and are responsible for the observed selective solid−gas adsorption properties toward H_2, N_2, and CO_2. At 77 K **1′** behaves as a molecular sieve, selectively adsorbing H_2 over N_2, possibly due to size-exclusion reasons. At variance, although CO_2 molecules are slightly larger than the pore size, they are readily incorporated by **1′** at temperatures as high as 433 K. Variable-temperature X-ray powder diffraction (TXRPD) studies, in the temperature range 303−473 K, show that dehydration is reversible and has almost negligible effects on the network. At variance, the uptake of CO_2 occurs through a transient phase and channels expansion. While the gas storage capacity of **1′** is not very high—H_2, 0.56 wt % and 0.010 kg H_2/L at 90 K and 900 Torr, and CO_2, 7.6 wt % at 273 K and 900 Torr—the guest molecules achieve very high densities, comparable to that of the liquid for H_2 (0.023 vs 0.021 molecules $Å^{-3}$) and to that of the solid for CO_2 (0.014 vs 0.022 molecules $Å^{-3}$). In addition, we have also studied the effect of the perturbation exerted by the guest molecules on its magnetic properties. The results show that while dehydration of **1** has negligible effect on its spin-canted antiferromagnetic behavior, CO_2 incorporation in the pores is responsible for an increment of the transition temperature at which the weak ferromagnetic ordering takes place from 22 to 29 K.

Introduction

Over the past 15 years, methodologies for the rational design of metal−organic frameworks (MOF's) and, particularly, porous coordination polymers (PCP's) have been the subject of extensive research[1] as results of their highly promising features for gas storage (e.g., H_2,[2] CO_2,[3] C_2H_2 [4]), selective separation,[5] and catalytic purposes.[6] Multiproperty materials of this kind,[7] which combine permanent porosity with additional properties such as chirality, framework flexibility, and magnetic or optical features, are, however, scarcer.

PCP's consist of metal ions connected through organic bridging ligands defining a porous network. In contrast to traditional porous species, such as zeolites and activated-carbon materials, PCP's have improved characteristic aspects that include (i) a framework responsible, as in dense solids, for physical properties such as magnetism, conductivity, and optical features,[8] (ii) well-ordered porous structures which may show flexible and dynamic behavior in response to guest molecules,[9]

† Departamento de Química Inorgánica, Universidad de Granada.
‡ Dipartimento di Chimica Inorganica, Metallorganica e Analitica, Università degli Studi di Milano.
§ Dipartimento di Chimica Strutturale e Stereochimica Inorganica, Università degli Studi di Milano and ISTM-CNR.
|| Instituto Nacional del Carbón, CSIC.
⊥ Dipartimento di Scienze Chimiche e Ambientali, Università dell'Insubria.

(1) See, e.g.: (a) Kitagawa, S.; Noro, S.-I.; Nakamura, T. *Chem. Commun.* **2006**, 701. (b) Férey, G.; Mellot-Draznieks, C.; Serre, C.; Millange, F.; Dutour, J.; Surble, S.; Margiolaki, I. *Science*, **2005**, *309*, 2040.
(2) Dinca, M.; Han, W. S.; Liu, Y.; Dailly, A.; Brown, C. M.; Long, J. R. *Angew. Chem., Int. Ed.* **2007**, *46*, 1419.
(3) Millward, A. R.; Yaghi, O. M. *J. Am. Chem. Soc.* **2005**, *127*, 17998.
(4) Matsuda, R.; Kitaura, R.; Kitagawa, S.; Kubota, Y.; Belosludov, R. V.; Kobayashi, T. C.; Sakamoto, H.; Chiba, T.; Takata, M.; Kawazoe, Y.; Mita, Y. *Nature* **2005**, *436*, 238.
(5) (a) Samsonenko, D. G.; Kim, H.; Sun, Y.; Kim, G.-H.; Lee, H.-S.; Kim, K. *Chem. Asian J.* **2007**, *1*, 484. (b) Ma, S.; Wang, X.-S.; Collier, C. D.; Manis, E. S.; Zhou, H.-C. *Inorg. Chem.* **2007**, *46*, 8499.
(6) (a) Dybtsev, D. N.; Nuzhdin, A. L.; Chun, H.; Bryliakov, K. P.; Talsi, E. P.; Fedin, V. P.; Kim, K. *Angew. Chem., Int. Ed.* **2006**, *45*, 916. (b) Wu, C.-D.; Hu, A.; Zhang, L.; Lin, W. *J. Am. Chem. Soc.* **2005**, *127*, 8940.
(7) e.g. (a) Kepert, C. J. *Chem. Commun.* **2006**, 695. (b) Bradshaw, D.; Claridge, J. B.; Cussen, E. J.; Prior, T. J.; Rosseinsky, M. J. *Acc. Chem. Res.* **2005**, *38*, 273. (c) Robin, A. Y.; Fromm, K. M. *Coord. Chem. Rev.* **2006**, *250*, 2127. (d) Maspoch, D.; Ruiz-Molina, D.; Veciana, J. *Chem. Soc. Rev.* **2007**, *36*, 770.

 10.1021/ja078074z CCC: $40.75 **© 2008 American Chemical Society**

Scheme 1. Schematic Representation of the Flexibility of the α Angles in Silicates and Metal−Pyrimidine Polymers, Respectively

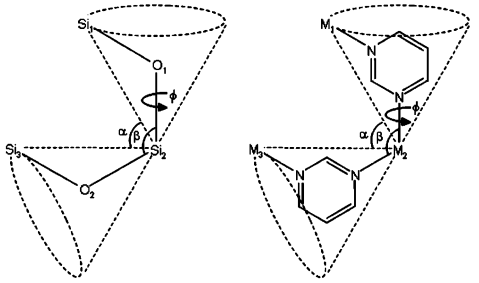

GEOMETRY	Tetrahedral	Tetrahedral	Square-planar
β	109.5°	109.5°	90°, 180°
α_{min} (ϕ = 0°)	74.5°	49.5°	30°, 120°
α_{max} (ϕ = 180°)	144.5°	169.5°	150°, 240°

and (iii) designable functionalities of the cavities surface, at the origin of their catalytic properties.[6,10]

However, it should be noted that the rational design and synthesis of MOF's with *zeolitic* networks, which are considered to be the most significant topologies for porous materials, are still a challenge. Metal imidazolates are one of the best known examples of zeolitic PCP's, as demonstrated by us[11] and others[12,13] by using different solvents and structure-directing agents (SDA's). In this context, also pyrimidines[14] and particularly pyrimidinolates,[15] which are very simple, angular and monovalent anions, can be used as synthones for obtaining zeomimetic materials (Scheme 1). Indeed, the different coordination geometry about the metal ion and the flexibility of the α angles (see Scheme 1) allow the formation of a variety of structural motives that can interlock so as to build a wide variety of zeolite-like structures.

In the recent past, we have reported the preparation and adsorption properties of sodalitic PCP's of the $[ML_2]_n$ type, containing square-planar Cu^{II} or Pd^{II} nodes and 5-X-pyrimidinolate linkers (X-pymo, X = H, halide).[16−18] Among the most intriguing materials of this class, the $[Pd(F\text{-pymo})_2]_n$ species[18b] should be highlighted as possessing unusually high thermal stability (370 °C in air) and remarkable H_2 storage capacity (0.018 kg H_2/L at 77 K and 900 Torr). In general, these polymers can be considered as metal−organic analogues of crystalline porous silica: $M(X\text{-pymo})_4$ primary building units (PBU's) generate $M_6(X\text{-pymo})_6$ and $M_4(X\text{-pymo})_4$ rings, as secondary building units (SBU's), which eventually combine into a 3-D framework resembling that of sodalite (SOD). At variance with the Pd^{II} counterpart,[18b] we have found that the introduction of the F residue as SDA at position 5 of the pyrimidinolate ring leads to the formation of a different zeotype, namely, the gismondine (GIS) PCP $[Cu(F\text{-pymo})_2(H_2O)_{1.25}]_n$ (**1**), built up from tetrahedrally distorted square-planar $Cu(F\text{-pymo})_4$ PBUs. In this paper, we present the synthesis and structural characterization of **1**. The remarkable solid−gas adsorptive properties of the "thermally activated" isomorphous counterpart (**1′**) and its guest-dependent magnetic properties are also discussed.

Experimental Section

General Methods. All the starting materials [5-fluoro-2-hydroxypyrimidine and $Cu(NO_3)_2{\cdot}3H_2O$] were purchased from Sigma-Aldrich and were used as received.

Preparation of $[Cu(F\text{-pymo})_2(H_2O)_{1.25}]_n$ (1). A water−ammonia (11:2) solution (10 mL) containing $Cu(NO_3)_2{\cdot}3H_2O$ (2 mmol, 0.48 g) was added dropwise to 5-fluoro-2-hydroxypyrimidine (4 mmol, 0.46 g) dissolved in 10 mL of water−ammonia (11:2) under stirring. The resulting solution afforded dark green crystals of **1** within 3 days. Yield: 95%. Anal. Calcd for $C_8H_{6.5}CuF_2N_4O_{3.25}$: C, 30.78; H, 2.10; N, 17.95. Found: C, 30.78; H, 1.96; N, 17.52.

Characterization and Physical Measurements. IR spectra were measured on a ThermoNicolet IR 200 spectrometer by using KBr pellets. Elemental (C, H, N) analyses were obtained at a Fisons-Carlo Erba EA 1008 analyzer (Center of Scientific Instrumentation, University of Granada, CIC); thermogravimetric analyses were recorded on Netzsch STA 409 PC Luxx (University of Insubria), at a heating rate of 10 K min^{-1} in the presence of a N_2 atmosphere. Adsorption isotherms were measured on a Micromeritics 2010 M (Instituto Nacional del Carbón, CSIC, Oviedo, Spain) and on a Micromeritics Tristar 3000 (University of Granada) volumetric instruments under continuous adsorption conditions. Prior to measurement, powder samples were heated at 303 K for 12 h and outgassed to 10^{-3} Torr using a Micromeritics Flowprep. The isosteric adsorption heats for CO_2 have been determined from the adsorption isotherms at two different temperatures (273 and 293 K) using the Clausius−Clapeyron equation. The CO_2 isobar was measured in the 298−473 K temperature range by means of a thermogravimetric balance, Shimadzu-TGA-50H (CIC), at a heating rate of 5 K min^{-1} in the presence of a CO_2 atmosphere; the polycrystalline sample was previously heated at 303 K for 12 h and outgassed to 10^{-3} Torr using a Micromeritics Flowprep. Magnetic susceptibility measurements were performed on polycrystalline samples in the 2−250 K with a quantum design MPMS XL squid (CIC) in the field-cooled mode applying 100, 300, and 5000 Oe. Ac magnetic susceptibility measurements were performed in the 2−30 K temperature range in a 1 Oe oscillating field at a frequency of 100 Hz. In the case of the magnetic measurements for the evacuated material **1′** and the CO_2-loaded species **1′@CO₂**, the as synthesized material **1** was heated at 303 K for 12 h and outgassed to 10^{-3} Torr using a Micromeritics Flowprep, this leading to **1′**. **1′** was loaded with CO_2 (1 bar) for 1 h to yield **1′@CO₂** and placed in a sealed tube.

(8) (a) Coronado, E.; Galán-Mascaros, J. R.; Gomez-Garcia, C. J.; Laukhin, V. *Nature*, **2000**, *408*, 447. (b) Maspoch, D.; Ruiz-Molina, D.; Wurst, K.; Domingo, N.; Cavallini, M.; Biscarini, F.; Tejada, J.; Rovira, C.; Veciana, J. *Nat. Mater*. **2003**, *2*, 190. (c) Niel, V.; Thompson, A. L.; Muñoz, M. C.; Galet, A.; Goeta, A. S. E.; Real, J. A. *Angew. Chem., Int. Ed.* **2003**, *42*, 3760. (d) Maspoch, D.; Ruiz-Molina, D.; Veciana, J. *J. Mater. Chem*. **2004**, *14*, 2713. (e) Olea, D.; Alexandre, S. S.; Amo-Ochoa, P.; Guijarro, A.; de Jesus, F.; Soler, J. M.; De Pablo, P. J.; Zamora, F.; Gomez-Herrero, J. *Adv. Mater*. **2005**, *17*, 1761.
(9) Kitagawa, S.; Kitaura, R.; Noro, S. I. *Angew. Chem., Int. Ed.* **2004**, *43*, 2334.
(10) (a) Lor, B. G.; Puebla, E. G.; Iglesias, M.; Monge, M. A.; Valero, C. R.; Snejko, N. *Chem. Mater*. **2005**, *17*, 2568. (b) Sato, T.; Mori, W.; Kato, C. N.; Yanaoka, E.; Kuribayashi, T.; Ohtera, R.; Shiraishi, Y. *J. Catal*. **2005**, *232*, 186. (c) Uemura, T.; Kitaura, R.; Ohta, Y.; Nagaoka, M.; Kitagawa, S. *Angew. Chem., Int. Ed.* **2006**, *45*, 4112.
(11) Masciocchi, N.; Bruni, S.; Cariati, E.; Cariati, F.; Galli, S.; Sironi, A. *Inorg. Chem.* **2001**, *40*, 5897.
(12) (a) Tian, Y.-Q.; Zhao, Y.-M.; Chen, Z.-X.; Shang, G.-N.; Weng, L.-H.; Zhao, D.-Y. *Chem.−Eur. J.* **2007**, *13*, 4146. (b) Huang, X.-C.; Lin, Y.-Y.; Zhang, J.-P.; Chen, X.-M. *Angew. Chem., Int. Ed.* **2006**, *45*, 1557.
(13) (a) Park, K. S.; Ni, Z.; Côté, A. P.; Choi, J. Y.; Huang, R.; Uribe-Romo, F. J.; Chae, H. K.; O'Keeffe, M.; Yaghi, O. M. *Proc. Natl. Acad. Sci. U.S.A.* **2006**, *103*, 10186. (b) Hayashi, H.; Côté, A. P.; Furukawa, H.; O'Keeffe, M.; Yaghi, O. M. *Nat. Mater*. **2007**, *6*, 501.
(14) (a) Keller, S. W.; Lopez, S. *J. Am. Chem. Soc*. **1999**, *121*, 6306. (b) Keller, S. W. *Angew. Chem., Int. Ed. Engl*. **1997**, *36*, 247.
(15) Navarro, J. A. R.; Barea, E.; Galindo, M. A.; Salas, J. M.; Romero, M. A.; Quirós, M.; Masciocchi, N.; Galli, S.; Sironi, A.; Lippert, B. *J. Solid State Chem*. **2005**, *178*, 2436.
(16) (a) Tabares, L. C.; Navarro, J. A. R.; Salas, J. M. *J. Am. Chem. Soc*. **2001**, *123*, 383. (b) Barea, E.; Navarro, J. A. R.; Salas, J. M.; Masciocchi, N.; Galli, S.; Sironi, A. *J. Am. Chem. Soc*. **2004**, *126*, 3014.
(17) Barea, E.; Navarro, J. A. R.; Salas, J. M.; Masciocchi, N.; Galli, S.; Sironi, A. *Polyhedron* **2003**, *22*, 3051.
(18) (a) Navarro, J. A. R.; Barea, E.; Salas, J. M.; Masciocchi, N.; Galli, S.; Sironi, A.; Ania, C. O.; Parra, J. B. *Inorg. Chem*. **2006**, *45*, 2397. (b) Navarro, J. A. R.; Barea, E.; Salas, J. M.; Masciocchi, N.; Galli, S.; Sironi, A.; Ania, C. O.; Parra, J. B. *J. Mater. Chem*. **2007**, *17*, 1939.

Table 1. Crystallographic Data and Structure Refinement Parameters for Species **1**

param	1
method	single-cryst XRD
formula	$C_8H_{6.5}CuF_2N_4O_{3.25}$
fw	312.21
T (K)	298(2)
λ (Å)	0.710 73
cryst system	tetragonal
space group	$I4_1md$
a (Å)	20.824(2)
c (Å)	10.0010(8)
V (Å^3)	4336.9(6)
Z	16
ρ(calcd) (Mg m^{-3})	1.913
μ (mm^{-1})	2.05
F(000)	2488
$S(F^2)^a$	1.025
R(F), wR(F^2) for $I > 2\sigma(I)^a$	0.048, 0.089
max, min $\Delta\rho$ (e Å^{-3})	0.51, −0.35

[a] $S(F^2) = [\Sigma w(F_o^2 - F_c^2)^2/(n - p)]^{1/2}$, where n is the number of reflections, p is the number of parameters and $w = 1/[\sigma^2(F_o^2) + (0.019P)^2 + 1.88P]$ with $P = (F_o^2 + 2F_c^2)/3$. $R(F) = \Sigma||F_o| - |F_c||/\Sigma|F_o|$ and $wR(F^2) = [\Sigma w(F_o^2 - F_c^2)^2/\Sigma wF_o^4]^{1/2}$.

Single-Crystal X-ray Diffractometry. A dark green crystal of species **1**, of approximate 0.10 × 0.10 × 0.10 mm dimensions, was glued on the tip of a glass fiber and mounted on top of a goniometric head. The data were collected at room temperature on a Bruker AXS APEX2 automated diffractometer (University of Milan) using graphite-monochromated Mo Kα radiation (λ = 0.710 73 Å) and setting the generator at 50 kV and 35 mA. The intensity data were collected within the limits $3.9 < 2\theta < 57.1°$ in the full sphere (ω scan method), with sample−detector distance fixed at 6 cm. A total of 1080 frames (40 s/frame; $\Delta\omega = 0.5°$) were measured affording a total of 19 515 reflections, of which 2904 unique and 2264 observed [$I > 2\sigma(I)$]. The unit cell was determined upon processing of the first 100 frames of each batch. The data were corrected for Lorenz−polarization and for absorption effects.[19] The structure solution was performed by direct methods (SIR-97).[20] The refinement was carried out by full-matrix least-squares procedures on F^2 (SHELX-97,[21] as implemented in the WinGX suite of programs), for 2264 data, 179 parameters, and 0 restraints. The analyzed crystal was a racemic twin (with a 0.42:0.58 components ratio). All the non-hydrogen atoms were treated anisotropically. The hydrogen atoms were made riding on the pertinent parent atoms with an isotropic thermal displacement parameter arbitrarily chosen as 1.2 times that of the parent atom itself. No hydrogen atoms were assigned to the oxygen atoms of the water molecules. Crystallographic data and structure refinement parameters are collected in Table 1. Crystallographic data (excluding structure factors) for species **1** have been deposited with the Cambridge Crystallographic Data Centre supplementary publication no. CCDC 653015. Copies of the data can be obtained free of charge on application to CCDC, 12 Union Road, Cambridge CB21EZ, U.K. (fax, (+44)1223-336-033; e-mail, deposit@ccdc.cam.ac.uk).

Variable-Temperature X-ray Powder Diffraction. Thermodiffractometric experiments were performed on microcrystalline batches of **1** on a Bruker AXS Advance D8 diffractometer (University of Milan), by employing a custom-made sample holder where both the environment and the temperature are under control (Officine Elettrotecniche di Tenno, Bleggio Inferiore, Italy). Typically, a sequence of scans in the 5−35° 2θ range was performed in the 303−473 K temperature range (each scan being acquired in isothermal conditions), heating (or cooling) in situ the sample in air or under CO_2 flow at ambient pressure. In air, a more accurate experiment was also performed in the 278−343 K range using a Peltier temperature controller, the other experimental conditions remaining unaltered. As for the experiments under CO_2, the transient phase was trapped and its behavior was monitored on cooling. This phase appears at about 363 K, with a concomitant lowering of peak intensity of the tetragonal phase and their coherent splitting into doublets (as required by symmetry decrease). On performing profile fitting on different peaks triplets, we estimated a ca. 60% maximum percentage for the elusive phase. Significantly, at RT (room temperature) and under a dynamic CO_2 flow, this phase disappears in about 45 min. Le Bail fits (Figure 1) of the diffractograms acquired (in air or under CO_2) were performed with the aid of Topas,[22] allowing us to estimate the temperature dependence of the lattice parameters. Typical values for the R_p and R_{wp} figures of merit of the Le Bail refinements lie in the range 0.097−0.119 (air), 0.030−0.036 (CO_2) and 0.134−0.172 (air), 0.042−0.047 (CO_2), respectively. As regards the transient phase, indexing was carried out manually upon observing the coherent splitting of many peaks of the tetragonal phase, clearly indicating a lowering in symmetry. The resulting orthorhombic cell (*Fdd*2; a = 29.13, b = 30.40, c = 9.89 Å; V = 8756.6 Å^3) may be alternatively described as rhombic (I lattice; a = 21.05, b = 21.05, c = 9.89 Å; γ = 92.44°; V = 4384.9 Å^3), thus better highlighting its structural relations to the pristine tetragonal phase.

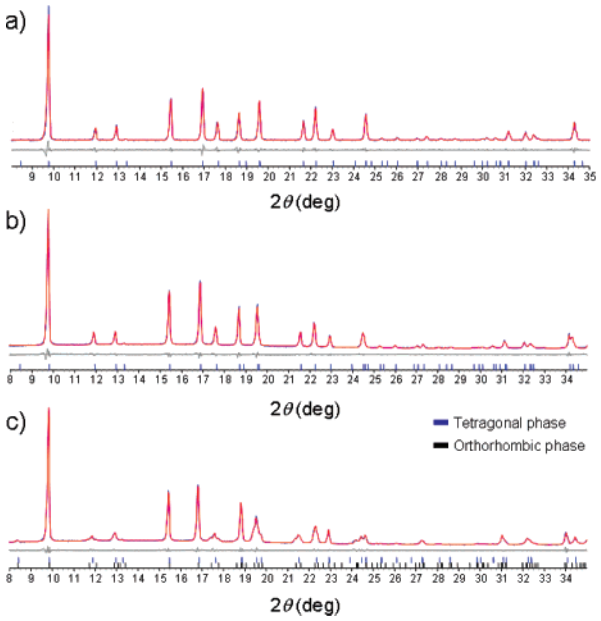

Figure 1. Typical graphical results of the Le Bail refinements performed on the TXRPD data with acquisitions (a) in air at 120 °C, (b) under CO_2 at 120 °C, and (c) under CO_2 at 50 °C (where both the tetragonal and the orthorhombic phases are present). Horizontal axis: 2θ angle, deg. Vertical axis: intensity, counts. Experimental, calculated, and difference profile: blue, red, and gray, respectively. The peak markers are shown at the bottom.

Results and Discussion

Crystal Structure. Crystals of **1** contain slightly distorted square-planar[23] Cu^{II} centers connected through N,N′-exobidentate F-pymo bridges [Cu−N 1.968(3)−1.976(3) Å]. The bridges define two different cyclic motives, namely metallacalix[8]-arenes and metallacalix[4]arenes exhibiting either an 1,3-alternate or a pinched cone conformation (Figure 2). In addition, four helical channels per *ab* square mesh (of 4_1 or 4_3 symmetry)

(19) SADABS, Sheldrick, G.; Blassing, B. *Acta Crystallogr.* **1995**, *A51*, 33.
(20) Altomare, A.; Burla, M. C.; Camalli, M.; Cascarano, G. L.; Giacovazzo, C.; Guagliardi, A.; Moliterni, A. G. G.; Polidori, G.; Spagna, R. *J. Appl. Crystallogr.* **1999**, *32*, 115.
(21) Sheldrick, G. M. *SHELX-97. Program for crystal structure determination*; University of Göttingen: Göttingen, Germany, 1997.
(22) *Topas-R, version 4: General profile and structure analysis software for powder diffraction data*; Bruker AXS: Karlsruhe, 2006.
(23) Average *trans*-N−Cu−N bond angle = 153.3°.

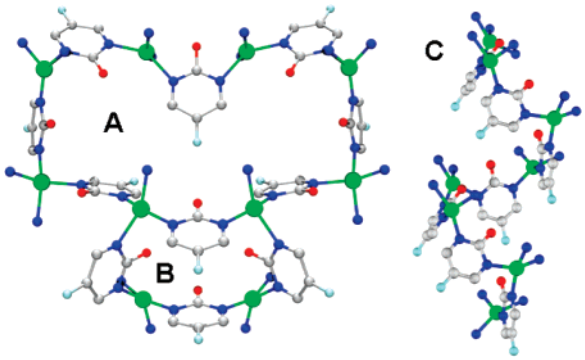

Figure 2. Basic structural motives found in **1**: metallacalix[8]arene (A); pinched cone metallacalix[4]arene (B); helix (C).

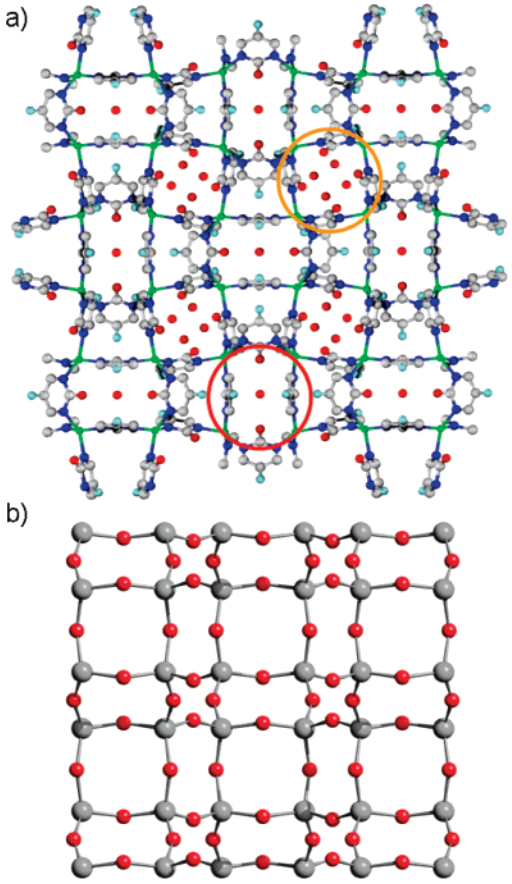

Figure 3. (a) View, down [001], of the crystal structure of **1**. The red and orange circles highlight one water-filled cavity and one helical channel, respectively. (b) Related gismondine skeleton.

run along *c* with an opening of about 2.9 Å (defined as the distance between atoms of opposite walls minus the pertinent van der Waals radii). The different structural motives interlock in a 3-D open framework related to the GIS zeotype (Figure 3). Noteworthy, the largest channels in classic GIS networks (eight-membered rings), running along *a* (and *b*), are hindered in **1** by the protruding F-pymo ligands, and only the "secondary" ones (helical channels) running along *c* are available for guest exchange. The polymeric network is further stabilized by extensive hydrogen bonding with the chlathrated water molecules. One of the crystallographically independent water molecules (O1) is located in the isolated cavities defined by one pinched cone metallacalix[4]arene and blocked by the one above and loosely interacts with the oxygen atoms of the

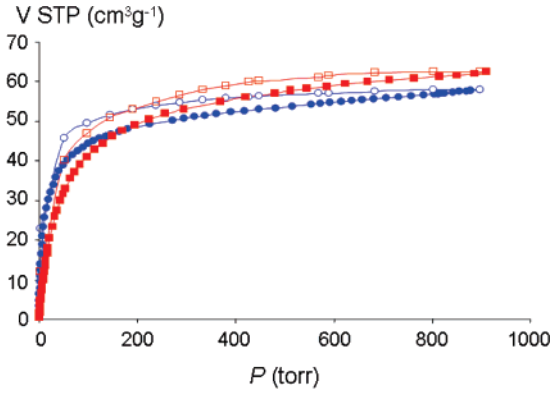

Figure 4. Hydrogen adsorption isotherms of **1′** at 77 (circles) and 90 K (squares). The open symbols denote desorption.

F-pymo ligands (O13 and O23; O1···O13 3.018 Å, O1···O23 3.170 Å). The second water molecule (O2) fills the helical channels and interacts with neighboring ones (O2···O2 2.991 Å) and with the F-pymo oxygen atoms decorating the pore walls (O2···O33 2.696 Å). The volume occupied by the chlatrated water molecules amounts to ca. 13% of the unit cell volume.[24]

Thermal Activation of 1. The thermal stability of **1** has been investigated by means of thermogravimetry (TG), differential scanning calorimetry (DSC), and variable-temperature X-ray powder diffraction (TXRPD) measurements. In the 313−473 K range, under a N_2 atmosphere, the TG trace of **1** shows a gradual weight-loss step of 6.7% (theoretical 7.2%), corresponding to the loss of the chlathrated water molecules, followed by a plateau from 473 to 513 K, indicating a relatively high thermal stability of the guest-free framework $[Cu(F\text{-}pymo)_2]_n$ (**1′**) which, according to XRPD, is isomorphous to **1**.

Gas Adsorption. The solid−gas adsorption properties of **1′** have been evaluated toward N_2 (77 K), H_2 (77 and 90 K), and CO_2 (273−473 K) to assess its textural properties (see Figures 4 and 5). Noteworthy, **1′** does not adsorb N_2; on the contrary, it adsorbs appreciable quantities of H_2 (0.56 wt % and 0.010 kg H_2/L at 90 K and 900 Torr) and CO_2 (7.6 wt % at 273 K and 900 Torr). The results at 77 K agree with a size-exclusion behavior of the 2.9 Å wide channels, which permits the diffusion of the small H_2 molecules over the N_2 ones (kinetic diameter: 2.89 Å vs 2.99 Å, respectively). At variance, the thermal energy of the marginally larger CO_2 molecules and of the coordination framework itself, in the 273−473 K temperature range, is high enough to widen the pore channels of **1′** permitting guests diffusion (see discussion below).

Regarding the H_2 adsorption, the isotherms measured at 77 and 90 K reveal an unusual behavior, i.e., the formation of hysteresis loops and the adsorption capacity at 90 K being similar to that measured at 77 K. The hysteretic desorption must be related to the structural features of **1′** and indicates a kinetic origin for the observed behavior. The adsorption kinetics are very slow (ca. 50 h for an adsorption−desorption cycle) and is likely linked to a hindered diffusion of the H_2 molecules through ultramicropores of comparable size. Given the close match between the pore size of the polymer and the kinetic dimensions of the adsorbate, the interaction potential of the H_2 molecules is expected to be very strong, due to the synergic effect of neighboring pore walls. Other authors have also attributed this

(24) Computed, upon removal of the guest molecules, using SMILE: Eufri, D.; Sironi, A. *J. Mol. Graphics* **1989**, *7*, 165.

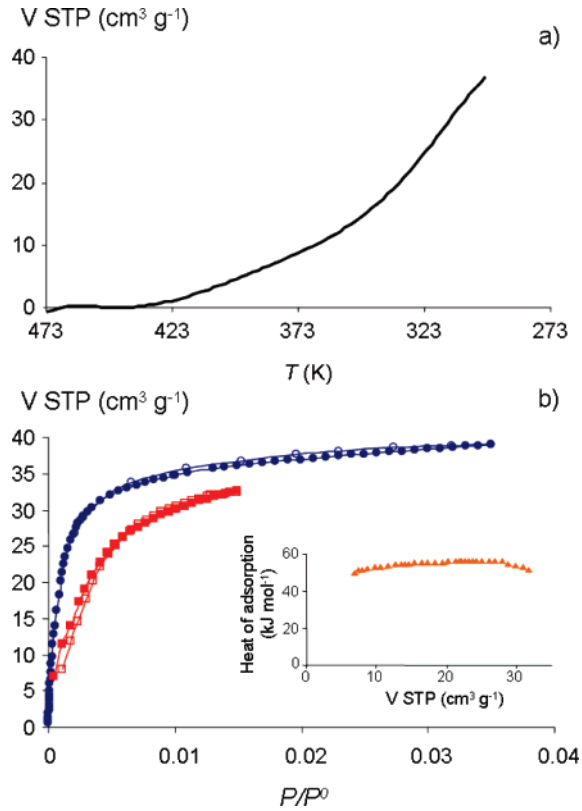

Figure 5. (a) CO_2 isobar of **1′** at 1 bar in the 298−473 K range. (b) CO_2 adsorption isotherm of **1′** at 273 K (circles) and 298 K (squares). The open symbols denote desorption. The inset shows the CO_2 adsorption enthalpy.

behavior to additional steric hindrance caused by adjacent guests (kinetic trapping).[25] Such slow desorption kinetics[25] might be the result of the high H_2 loading of the porous framework at low pressures, which impedes the flexibility and window-opening.

As mentioned above, CO_2 molecules are slightly larger (3.189 Å) than the pore opening; however, the isotherms at 273 and 293 K are fully reversible and of type I (see Figure 5b). This is in agreement with the higher kinetic energy of these guest molecules, coupled to a certain flexibility of the porous framework at higher temperatures (see below).[26] The isotherm at 273 K is also consistent with the typical behavior of a molecular sieve, with a steep slope at very low pressures indicative of pores of small size.

The isosteric heats of CO_2 adsorption were evaluated according to the Clausius−Clapeyron eq 1 from the adsorption isotherms measured at 273 and 293 K (Figure 5b):

$$q_{st} = -R\left(\frac{d(\ln P)}{d(1/T)}\right)_N \qquad (1)$$

Here q_{st}, R, P, and N represent isosteric heat of adsorption, gas constant, pressure, and amount of adsorption of CO_2, respectively. The CO_2 molecules strongly interact with the host, the adsorption heat (49−55 kJ mol^{-1}) being considerably higher than in other porous coordination polymers and close to those exhibited by zeolites.[27] The strong interaction of **1′** toward CO_2

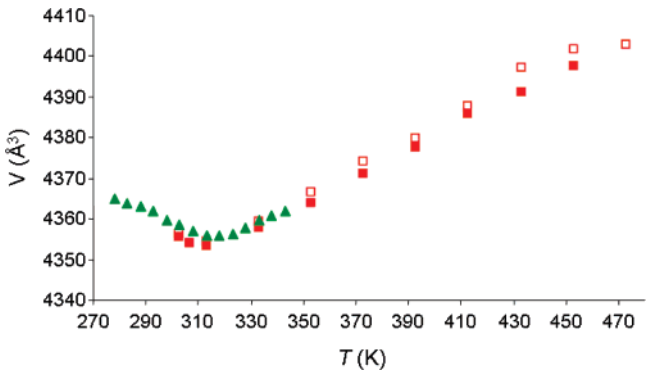

Figure 6. Variations of the unit cell volume of **1** in air in the 303−473 K range: open red squares, heating; full red squares, cooling; green triangles, finely sampled cooling branch in the 278−343 K range.

is further supported by what is emerging from the CO_2 isobar measured at P_{CO_2} = 1 bar in the 473−298 K temperature range: on lowering of the temperature, **1′** uptakes this gas below 428 K (Figure 5a).

Noteworthy, given the small volume available for guest exchange in **1′** (ca. 13%), the densities of H_2 and CO_2 stored in the cavities of **1′** are very high, comparable to that of the liquid for H_2 (0.023 vs 0.021 molecules Å^{-3}) and to that of the solid for CO_2 (0.014 vs 0.022 molecules Å^{-3}).[28] This type of unusually high guest density has been previously observed by Kitagawa et al. on C_2H_2 (0.010 molecules Å^{-3}),[4] N_2 (0.024 molecules Å^{-3}), O_2 (0.024 molecules Å^{-3}), and CO_2 (0.024 molecules Å^{-3})[26] in ultramicroporous coordination networks. With these numbers in mind, to our knowledge, **1′** is one of the best performing materials *in terms of H_2 density*,[29] surpassed only by the $Mg_3(HCO_2)_6$ species, for which a H_2 density of 0.042 molecules Å^{-3} can be calculated.[30]

Thermodiffractometric (TXRPD) Studies. Given the small volume available for guest exchange in **1′**, these remarkable adsorption properties are rather surprising. Due to the well-known flexibility of GIS frameworks,[31] we initially suspected an expansion/shrinkage dynamic behavior triggered by gas adsorption/desorption.[32] To verify this hypothesis we performed different thermodiffractometric experiments, in the 303−473 K temperature range, under different environments (air, N_2, and CO_2).

On heating of the sample in air in the 303−473 K temperature range, the cell volume unexpectedly shows a minimum at 313 K, after which a smooth volume increase is observed (ca. 1%, Figure 6). The same trend has been observed in a more accurate experiment (see the Experimental Section for further details) in the 278−343 K range. The values determined upon heating match almost perfectly those observed upon cooling, thus sustaining the full reversibility of the dehydration process (Figure 6). Combining this XRPD evidence with that from the thermal analysis, we may ascribe the observed volume shrinking to the early partial loss of chlatrated water molecules, while the subsequent volume increase is possibly due to thermal

(25) Zhao, X.; Xiao, B.; Fletcher, A. J.; Thomas, K. M.; Bradshaw, D.; Rosseinsky, M. J. *Science* **2004**, *306*, 1012.
(26) Kitaura, R.; Matsuda, R.; Kubota, Y.; Kitagawa, S.; Takata, M.; Kobayashi, T. C.; Suzuki, M. *J. Phys. Chem. B* **2005**, *109*, 23378.
(27) Bourrelly, S.; Llewellyn, P. L.; Serre, C.; Millange, F.; Loiseau, T.; Férey, G. *J. Am. Chem. Soc.* **2005**, *127*, 13519.
(28) Simon, A.; Peters, K. *Acta Crystallogr., Sect. B* **1980**, *36*, 2750.
(29) Collins, D. J.; Zhou, H.-V. *J. Mater. Chem.* **2007**, *17*, 3154.
(30) Rood, J. A.; Noll, B. C.; Henderson, K. W. *Inorg. Chem.* **2006**, *45*, 5521.
(31) Allen, S.; Carr, S.; Chapple, A.; Dyer, A.; Heywood, B. *Phys. Chem. Chem. Phys.* **2002**, *4*, 2409 and references therein.
(32) Kondo, A.; Noguchi, H.; Ohnishi, S.; Kajiro, H.; Tohdoh, A.; Hattori, Y.; Xu, W.-C.; Tanaka, H.; Kanoh, H.; Kaneko, K. *Nano Lett.* **2006**, *6*, 2581.

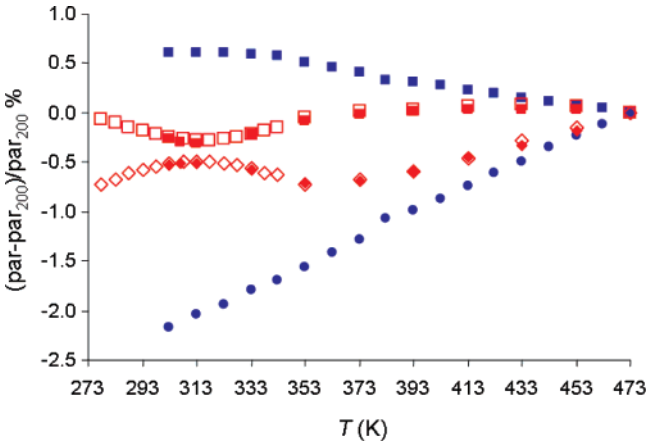

Figure 7. Relative variations of the unit cell parameters (*a* and *c* axes, squares and circles, respectively) of **1** in the 303−473 K range, in air (red symbols) and under CO_2 (blue symbols). All parameters have been normalized to their 473 K value. Full symbols indicate data collected on cooling.

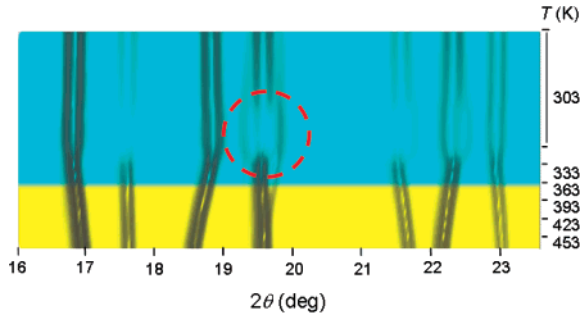

Figure 8. 2D plot representing the variable-temperature X-ray powder diffraction traces of **1′** acquired under a CO_2 flow. Horizontal axis: 2θ range (deg). Vertical axis: temperature acquisition range (a number of scans were performed on cooling from 473 K, while the latter part of the experiment was carried out at 303 K; see the Experimental Section for further details). Cyan: coexistence of the tetragonal and orthorhombic transient phases. The red circle highlights one example of the lowering of peak intensity of the tetragonal phase with its coherent splitting into doublets. The transient phase has substantially disappeared at the end of the experiment.

Scheme 2. Structural Modifications in the $[Cu(F\text{-}pymo)_2]_n$ Framework upon CO_2 Inclusion

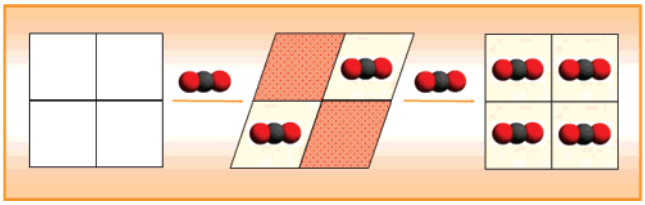

expansion effects overcoming the loss of the remaining water molecules. On the whole, as also witnessed by the thermal analysis, the dehydration process occurs smoothly, without the formation of intermediate (amorphous or crystalline) phases.

Taking into account the relative changes experienced by the lattice parameters in air, this porous framework undergoes a limited stress during heating and dehydration. In this regard, the computed maximum value of 7×10^{-5} K^{-1} for $\delta(\ln V)/\delta T$, even if higher than those of rigid materials of this kind [see, e.g., 5.3×10^{-6} K^{-1} for the extremely stiff $Pd(F\text{-}pymo)_2$],[18b] falls below those of soft molecular (i.e., nonpolymeric) materials (e.g., 2.2×10^{-4} K^{-1} for solid sulfur or 4.8×10^{-4} K^{-1} for glycerine[33]).

At variance, with sample cooling under a CO_2 flow, there is a tradeoff between lattice parameters at temperatures below 413 K, which favors CO_2 diffusion: *a* and *b* lengthen while *c* shortens (Figure 7), with a consequent widening (in the *ab* plane) of the four unit cell helical channels. Moreover, during cooling, a transient phase, coexisting with the tetragonal one, is detected below 363 K (Figure 8). Its lower symmetry (see Experimental Section) suggests a different behavior of the four helical channels toward CO_2 exchange, i.e., some specialization and cooperativity of CO_2 adsorption (see below).

We suppose that, below 363 K, settling of the "previously" adsorbed CO_2 molecules starts—the CO_2 isobar is indicative of the adsorption of 2.3 CO_2 molecules/unit cell at 363 K. Indeed, the transient phase speaks for a rhombic distortion of the *ab* square mesh coherent with an *early*, preferential "freezing" of CO_2 in (two, isochiral) diagonally related channels. *Later on*, when "freezing" occurs also in the other (two) channels of opposite chirality, the original tetragonal lattice is restored (Scheme 2).

The strong interaction of the CO_2 molecules with the pore walls may be related to feasible interaction of this quadrupolar molecule with the polarizing O and F residues. In this regard, we have previously found that the introduction of a F residue in the isoreticular SOD $[Pd(X\text{-}pymo)_2]_n$ frameworks (X = H, F) significantly enhances CO_2 adsorption.[18b]

Magnetic Properties. We have studied the effect of the perturbation exerted by the guest molecules on the $[Cu(F\text{-}pymo)_2]_n$ network on its magnetic properties. With this purpose we have measured the thermal behavior of the magnetic susceptibility for the as synthesized, hydrated material $[Cu(F\text{-}pymo)_2(H_2O)_{1.25}]_n$ (**1**), the activated material $[Cu(F\text{-}pymo)_2]_n$ (**1′**), and the latter loaded with CO_2 (**1′@CO₂**) (Figure 9). The high-temperature behavior of the dc magnetic susceptibility (χ_M) of **1** is typical of an antiferromagnetic material, with a maximum at about 60 K and a smooth decrease of the $\chi_M T$ values from 0.222 cm^3 mol^{-1} K at 250 K to 0.046 cm^3 mol^{-1} K at 24 K. This behavior is due to antiferromagnetic coupling of the copper(II) centers transmitted through the N,N′-F-pymo bridges. However, below the Néel temperature T_N ca. 24 K, χ_M and $\chi_M T$ sharply increase.[34] The sharp increment of the χ_M and $\chi_M T$ values in the low-temperature region and at low field strengths suggests a weak ferromagnetic ordering arising from a spin-canting phenomenon. The origin of this behavior can be traced back to the noncentrosymmetric nature of the framework,[35] which allows an antisymmetric effect to be present, originated from a small ferromagnetic interaction. The overall behavior of the activated form **1′** is very similar to that of the as-synthesized material **1**; however, a slight diminution (2 K) of the temperature at which the weak ferromagnetic ordering takes place is observed. It is noteworthy that the loading of the material with carbon dioxide has a more profound effect on its magnetic properties. In this case, we observe an increase of ca. 6 K in the temperature corresponding to the maximum of the magnetic susceptibility (χ_M) curve. Likewise, the temperature

(33) Perry, R. H.; Green, D. W.; Maloney, J. O. Eds. *Perry's Chemical Engineers' Handbook*, 7th ed.; McGraw Hill: New York, 1998; Tables 2-147.

(34) The presence of a weaker additional magnetic ordering taking place below 17 K should also be noted.

(35) Kahn, O. *Molecular Magnetism*; Wiley-VCH: New York, 1993.

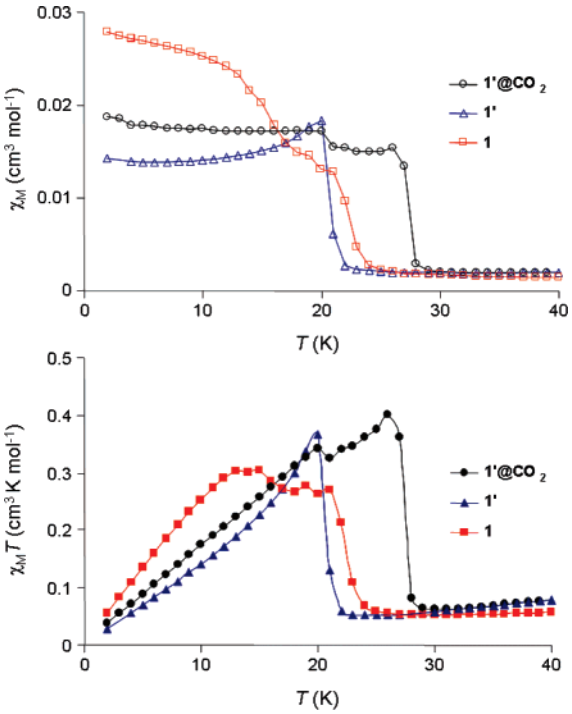

Figure 9. Effect of the guest molecules in the magnetic behavior of $[Cu(F\text{-}pymo)_2]_n$ at an external magnetic field of 100 Oe: as-synthesized hydrated $[Cu(F\text{-}pymo)_2(H_2O)_{1.25}]_n$ (**1**, red squares); activated $[Cu(F\text{-}pymo)_2]_n$ (**1′**, blue triangles); loaded with CO_2 (**1′**@CO_2, black circles).

at which the weak ferromagnetic ordering appears increases by ca. 5 and 7 K compared to **1** and **1′**, respectively. The perturbation of the magnetic properties induced by guest incorporation can be traced back to the thermal XRPD structural studies (see above) which show that the incorporation or release of water molecules has little effect on the $[Cu(F\text{-}pymo)_2]_n$ network compared to the incorporation of CO_2 guest molecules, which is responsible for a significant framework distortion. It is noteworthy that there are few cases in which a related vapo−magnetic/solvato−magnetic effect have been observed: dehydration/desolvation on spin-crossover transitions[36] or changes in the magnetic properties upon loading or release of small alcohol molecules have been reported.[8b] Related to this, we have previously observed that the incorporation of ion pairs in the $[Cu(2\text{-}pymo)_2]_n$ pyrimidinolate PCP leads to a profound structural reorganization from a 3D SOD framework[16a] to a layered muscovite type material,[37] with concomitant apparition of a spin-canting phenomenum. However, the effect of CO_2 incorporation on the magnetic properties of **1′** framework is a rare example (apart from SCO materials) of a gas sensitive magnetic behavior in which only the outer spin environment, not the inner one, is dramatically altered. In this regard, we presume that the structural perturbation exerted by the CO_2 guests may lead to a less distorted square planar CuN_4 environment with a concomitant larger overlapping of the orbitals of the bridging F-pymo ligands and the copper(II) $d_{x^2-y^2}$ magnetic orbitals, which permits a more efficient magnetic exchange.

Conclusions

The results presented here further support the rich variety of physicochemical properties exhibited by the metal pyrimidinolates, ranging among high thermal stability, molecular recognition, and unusual magnetic properties. Moreover, this contribution confirms the remarkable properties of ultramicroporous coordination networks which, although lacking of large capacities, show very high gas storage densities and guest selectivity. Our experiments also reveal that the performance of the $[Cu(F\text{-}pymo)_2]_n$ PCP as a semirigid network—as evidenced by its behavior as a molecular sieve of H_2 over N_2 and the minimal stress on the network exerted by dehydration and thermal treatments—is modified when exposed to CO_2. The uptake process of CO_2 is responsible for the expansion of the pores and the formation of a transient phase with selective and cooperative ordering of the guests, well before complete filling of the pores occurs. Moreover, it is noteworthy that the structural perturbation exerted by the CO_2 molecules can tune the magnetic properties of the $[Cu(F\text{-}pymo)_2]_n$ network. Indeed, the observed gas sensitive, long-range magnetic ordering in a porous material where the inner metal environment is not substantially altered is highly remarkable. Finally, it should be highlighted that the use of different metal ions and the introduction of diverse substituents in the pyrimidinolate ligands have allowed us to tune the structural, magnetic, and gas-adsorption properties of the isolated PCP's.

Acknowledgment. We thank the reviewers for their helpful comments and the support by the Spanish and Italian Ministries of Education and Science for the projects CTQ2005-00329/BQU, HI2006-0116, and PRIN 2006: "Materiali ibridi metallo-organici multifunzionali con leganti poliazotati". We also acknowledge financial support by the Fondazione CARIPLO. Postdoctoral grants MEC-EX2004-0612 (E.B.) and Fundación Ramón Areces (A.R-D.) are also acknowledged.

JA078074Z

(36) (a) Halder, G. J.; Kepert, C. J.; Moubaraki, B.; Murray, K. S.; Cashion, J. D. *Science*, 2002, *298*, 1762. (b) Bonhommeau, S.; Molnar, G.; Galet, A.; Zwick, A.; Real, J. A.; McGarvey, J. J.; Bousseksou, A. *Angew. Chem., Int. Ed*. 2005, *44*, 4069. (c) Galet, A.; Muñoz, M. C.; Real, J. A. *Chem. Commun*. 2006, 4321.

(37) Navarro, J. A. R.; Barea, E.; Salas, J. M.; Masciocchi, N.; Galli, S.; Sironi, A.; Ania, C. O.; Parra, J. B. *Inorg. Chem.* **2007**, *46*, 2988.